Available online at www.sciencedirect.com
ScienceDirect
Journal of Colloid and Interface Science 308 (2007) 142–156
JOURNAL OF Colloid and Interface Science
www.elsevier.com/locate/jcis

Comparative characterization of polymethylsiloxane hydrogel and silylated fumed silica and silica gel

V.M. Gun'ko [a,*], V.V. Turov [a], V.I. Zarko [a], E.V. Goncharuk [a], I.I. Gerashchenko [a], A.A. Turova [a], I.F. Mironyuk [b], R. Leboda [c], J. Skubiszewska-Zięba [c], W. Janusz [c]

[a] *Institute of Surface Chemistry, 17 General Naumov Street, Kiev 03164, Ukraine*
[b] *Pricarpatsky Stefanyk University, 57 Shevchenko Street, Ivano-Frankovsk, Ukraine*
[c] *Faculty of Chemistry, Maria Curie-Skłodowska University, 20031 Lublin, Poland*

Received 10 October 2006; accepted 16 December 2006

Available online 25 January 2007

Abstract

Polymethylsiloxane (PMS) hydrogel ($C_{PMS} = 10$ wt%, soft paste-like hydrogel), diluted aqueous suspensions, and dried/wetted xerogel (powder) were studied in comparison with suspensions and dry powders of unmodified and silylated nanosilicas and silica gels using ^{1}H NMR, thermally stimulated depolarization current (TSDC), quasielastic light scattering (QELS), rheometry, and adsorption methods. Nanosized primary PMS particles, which are softer and less dense than silica ones because of the presence of CH_3 groups attached to each Si atom and residual silanols, form soft secondary particles (soft paste-like hydrogel) that can be completely decomposed to nanoparticles with sizes smaller than 10 nm on sonication of the aqueous suspensions. Despite the soft character of the secondary particles, the aqueous suspensions of PMS are characterized by a higher viscosity (at concentration $C_{PMS} = 3$–5 wt%) than the suspension of fumed silica at a higher concentration. Three types of structured water are observed in dry PMS xerogel (adsorbed water of 3 wt%). These structures, characterized by the chemical shift of the proton resonance at $\delta_H \approx 1.7$, 3.7, and 5 ppm, correspond to weakly associated but strongly bound water and to strongly associated but weakly or strongly bound waters, respectively. NMR cryoporometry and QELS results suggest that PMS is a mesoporous–macroporous material with the textural porosity caused by voids between primary particles forming aggregates and agglomerates of aggregates. PMS is characterized by a much smaller adsorption capacity with respect to proteins (gelatin, ovalbumin) than unmodified fumed silica A-300.

Keywords: Polymethylsiloxane hydrogel; Silylated fumed silica; Silica gel; Aqueous suspension; Structured water; Morphology; Structural characteristics; ^{1}H NMR; TSDC; QELS; Rheometry; Protein adsorption

1. Introduction

Polymethylsiloxane (PMS) materials have drawn considerable fundamental and technological interest because of their applications as components of nanocomposites [1–3], copolymers for synthesis of ion-conducting polymeric materials [4–11]. PMS is used in chromatography [12–14], e.g., for coating of a silica surface [15], and in medicine as a component of medicinal preparations (e.g., Cleocin, Universal Washaid, USA), implants, adjuvant Capsil (Aquatrols, USA; Scotts, USA), a vaccine adjuvant [16], etc. Additionally, PMS in the form of soft pastelike hydrogel ($C_{PMS} \approx 10$ wt%) is utilized as a medicinal enterosorbent, Enterosgel (Kreoma-Pharm, Ukraine) [17,18]. Functionalized PMSs [19,20] are used for modification and functionalization of solid surfaces [21,22]. They are also used as supports for catalysts [23] or as polymer backbones for preparation of liquid crystalline polymers [24,25]. NMR investigations and dielectric relaxation measurements show a strong dependence of the mobility of polysiloxanes on the structure of side groups [26]. This structure determines the shear elasticity of polymers [17,18,27] and other characteristics. Despite numerous investigations of polysiloxane materials (the lion's share of them are related to linear polysiloxanes such as polydimethylsiloxanes, PDMS), the behavior of interfacial water in xerogels, hydrogels, and aqueous suspensions of branched PMS

* Corresponding author. Fax: +380 44 424 3567.
E-mail address: gun@voliacable.com (V.M. Gun'ko).

0021-9797/$ – see front matter
doi:10.1016/j.jcis.2006.12.053

is practically not studied, especially in comparison with that in silylated nanosilica possessing close specific surface area, the same surface functionalities but differently composed, and different particle morphology.

Branched PMS can be synthesized using different precursors X_3SiCH_3, where X = Cl, OR, etc. Three reactive X groups hydrolyzed provide cross-linking, in contrast to linear PDMS synthesized using $X_2Si(CH_3)_2$. The properties of PMS materials in different forms (hydrogels, xerogels, dry powders, etc.) depend on the cross-linking degree, which is maximal in dry xerogel (hydrophobic), in which all the Si atoms are bonded by three siloxane bonds ($\equiv$Si–O)$_3$SiCH$_3$, and on the hydration degree. Heating/drying of PMS hydrogels can lead to loss of the hydrophilic properties because of enhancement of cross-linking by the Si–O–Si bonds on condensation of hydrophilic silanols [28]. Heated PMS xerogel with the maximal cross-linking degree is practically hydrophobic and not wetted by water (contact angle >95°). However, PMS hydrogel can retain significant amounts of water and its aqueous suspension is stable for a long time because of incomplete cross-linking and the presence of residual hydrophilic silanols [17,18,28]. The PDMS-silica contact distance is decreased as the level of water (both chemisorbed and physisorbed) in the interfacial region is decreased. In addition, water in the interfacial region seems to screen the long-range interactions, mediating the polymer relaxation dynamics and ultimately increasing the polymer mobility [29]. There are several water structures (types) adsorbed on PDMS/silica composite, desorption of which can be separated depending on temperature of desorption [30].

The hydrophilic–hydrophobic properties of the PMS hydrogel and xerogel surfaces can be close to those of partially and completely silylated fumed silica, respectively [31–36] because these materials have close specific surface area (200–300 m^2/g) and the same surface functionalities ($\equiv$SiCH$_3$, $\equiv$SiOH, and $\equiv$Si–O–Si$\equiv$) and are characterized by textural porosity (i.e., voids between particles nondensely packed in secondary structures). The hydrophobic functionalities (trimethylsilyl, TMS, or dimethylsilyl, DMS) on a silylated silica surface inhibit formation of a continuous layer of adsorbed water [33]. Therefore, one can expect clusterization of interfacial water in PMS hydrogel or water adsorbed on PMS xerogel. Comparison of the adsorption characteristics of unmodified and differently modified silicas [33–36] shows that even partial silylation of the silica surface reduces the adsorption of water by several times. Nevertheless, partially or completely silylated nanosilica placed in an aqueous medium can disturb a relatively thick layer of interfacial water [33,35,36]. A similar effect can be expected for PMS hydrogel and suspension. However, the differences in the structure of primary particles of PMS [17,18,28] and silylated fumed silica [31,37], as well as in the composition of surface sites (($\equiv$Si–O)$_3$SiCH$_3$ and ($\equiv$Si–O)$_2$Si(OH)CH$_3$ for PMS and $\equiv$Si–OSi(CH$_3$)$_3$ and ($\equiv$Si–O)$_2$Si(CH$_3$)$_2$ for TMS- and DMS-nanosilica, respectively), can lead to certain differences in the behavior of bound water, as well as in the physicochemical characteristics of concentrated and diluted aqueous suspensions, hydrogels, and dry powders with these materials. Wetting/drying of nanosilica, which is composed of rigid primary particles forming nonrigid aggregates and agglomerates of aggregates, changes both structural and morphological characteristics of the powder [37,38]. Similar effects caused by transformation of PMS hydrogel (composed of soft primary and secondary particles) into xerogel can be stronger than those for fumed silica because of the enhancement of the cross-linking degree in dried PMS particles.

To analyze the effects of the liquid media on rigid and soft materials, such techniques as NMR cryoporometry [33,39–41], thermally stimulated depolarization current (TSDC) [33,42], and quasielastic light scattering (QELS) can be used without removal of the liquids (i.e., as nondestructive methods) in combination with standard adsorption [33,42] and other methods applied to both aqueous dispersions and dry powders. The aim of this work is to analyze regularities in the structural and adsorption characteristics of PMS in the forms of suspension, hydrogel, and xerogel compared with those of aqueous suspensions and dry powders of unmodified and silylated fumed silica and silica gel using ^{1}H NMR and TSDC with layer-by-layer freezing-out of bulk and interfacial water, QELS, rheometry, and adsorption of proteins.

2. Materials and techniques

2.1. Materials

Commercial polymethylsiloxane hydrogel (Kreoma-Pharm, Kiev, Ukraine) synthesized using methyltrichlorsilane [17,18,28] including 10 wt% of PMS and 90 wt% of water (homogeneous soft dough, paste-like hydrogel in which all water is bound in pores) was used as the initial material. For NMR investigations, the aqueous suspensions of PMS (C_{PMS} = 1.25, 2.5, and 5 wt%) were prepared by dilution of the initial PMS hydrogel with distilled water. Dry PMS xerogel ($C_{PMS} \approx$ 97 wt%) was obtained from the initial material dried in air at 300 K for five days. PMS xerogel wetted by ethanol and then ethanol/water and repeatedly washed off with water contains approximately 72 wt% of water.

Fumed silicas A-300 and A-380 (pilot plant of the Institute of Surface Chemistry, Kalush, Ukraine) at the specific surface areas $S_{BET} \approx$ 337 and 378 m^2/g, respectively, were silylated by dymethyldichlorosilane (C_{DMS} = 0.24, 0.57, 0.84, 1.12, and 1.21 mmol/g) and hexamethyldisilazane, HMDS (C_{TMS} = 0.09, 0.14, 0.12, 0.23, 0.42, and 0.79 mmol/g), respectively. The structural and other characteristics of silylated A-380 samples were described in detail elsewhere [35].

Structural characteristics of unmodified silica gels Si-40, Si-60, and Si-100 (Merck) and silylated Si-60 (approximately 30% OH groups in silanols were replaced by TMS groups in reaction of silica with HMDS) used here in comparative investigations and the behavior of pore water in these silica gels are described in detail elsewhere [33,42–44].

2.2. ^{1}H NMR

For recording ^{1}H NMR spectra of water bound to the silica and PMS surfaces, a high-resolution WP-100 SY (Bruker)

NMR spectrometer with a bandwidth of 50 kHz was used. Relative mean errors were ±10% for signal intensity and ±1 K for temperature. The characteristics of bound (structured, unfrozen) water were determined from the intensity of the ^{1}H NMR spectra recorded at $T < 273$ K. Concentration of unfrozen water as a function of temperature ($C_{uw}(T)$) was determined by comparison of the integral intensities of the ^{1}H NMR signals of unfrozen water at given temperatures and liquid water at 285 K [33]. The ^{1}H NMR signals of water molecules from ice, functionalities of PMS, surface TMS, DMS, and silanols do not contribute to the ^{1}H NMR spectra because of features of the measurement technique and the short time ($\sim 10^{-6}$ s) of transverse relaxation of protons in immobile structures, which is shorter by several orders of magnitude than that of mobile water molecules. This method and its applications to different materials are described in detail elsewhere [33].

Water can be frozen in narrower pores at lower temperatures that can be described by the Gibbs–Thomson (GT) relation for freezing point depression for pore liquids [39–41],

$$\Delta T_m = T_{m,\infty} - T_m(R) = -\frac{2\sigma_{sl} T_{m,\infty}}{\Delta H_f \rho R} = \frac{k}{R}, \tag{1}$$

where $T_m(R)$ is the melting temperature of ice in pores of radius R, $T_{m,\infty}$ is the bulk melting temperature, ρ is the density of the solid, and σ_{sl} the energy of solid–liquid interaction. Equation (1) can be transformed into the integral equation (IGT) [45,46]

$$C_{uw}(T_m) = A \int_{R_{min}}^{R_{max}} \left(\frac{k}{(T_{m,\infty} - T_m(R))R} \right)^2 f_V(R)\, dR, \tag{2}$$

where R_{max} and R_{min} are the maximal and minimal pore radii (or sizes of unfrozen liquid structures), respectively, and A is a normalization factor. The IGT equation was solved using modified CONTIN [47] or CONTIN/maximum entropy method (MEM) [45,46,48] procedures.

The pore size distribution (pores filled by structured water) can be calculated directly with Eq. (1) using the dependence of the amount of unfrozen water on temperature (C_{uw} as a function of T determined as changes in the ^{1}H NMR signal of unfrozen water at this temperature) and pore size (R) as a function of $T_m(R)$ that gives changes in C_{uw} as a function of R. Calculations with the integral equation (2) give the distribution function $f(R)$, which can differ from that calculated directly, because solution of Eq. (2) is a well-known ill-posed problem due to the impact of noise on measured data, and the regularization procedure, especially in the case of application of the maximum entropy principle to this function, gives a clean, more exact solution than that on direct calculations with Eq. (1) because noise effects are reduced.

The $f(R)$ distribution was used to calculate the contributions of micropores ($R < 1$ nm), mesopores ($1 < R < 25$ nm) and macropores ($R > 25$ nm) to the total porosity,

$$V = \int_{R_{min}}^{R_{max}} f(R)\, dR, \tag{3}$$

where R_{min} and R_{max} correspond to the integration ranges for the mentioned types of pores. Additionally, this $f(R)$ function related to pore volume ($f_V(R)$) can be converted to $f_S(R)$ related to the specific surface area using the corresponding model of the pore shape,

$$f_S(R) = \frac{w}{R}\left(f_V(R) - \frac{V(R)}{R} \right), \tag{4}$$

where $w = 1, 2$, and 1.36 for slit shaped and cylindrical pores and voids between spherical particles packed in the cubic lattice, respectively. Integration of the $f_S(R)$ function gives the specific surface area (S_{IGT}) of the studied materials in contact with structured water, which can be divided into the corresponding pore ranges as was done for the pore volume.

2.3. QELS

Quasielastic light scattering (QELS) measurements of the particle size distributions [37,38] were performed using a Zetasizer 3000 (Malvern Ins., $\lambda = 633$ nm, scattering angle 90°, software version 1.4). A PMS suspension at $C_{PMS} = 1$ wt% was prepared with the initial commercial hydrogel ($C_{PMS} = 10$ wt%) diluted with twice-distilled deionized water (pH 6.72, conductivity <2 μS cm^{-1}) and sonicated by a Sonicator Misonix (USA) ultrasonic disperser (22 kHz, 500 W) for 5 min. PMS suspensions with lower concentrations of PMS were prepared by dilution of this suspension ($C_{PMS} = 1$ wt%) to $C_{PMS} = 0.25, 0.0625, 0.0156$, and 0.0078 wt% and then sonicated for 1 min. The particle size distributions are shown here with respect to the scattered light intensity, which was also recalculated to the size distribution related to the particle number and the particle volume using the Malvern software. The value of the effective diameter of particles (D_{eff}) is the average value, which can be used to characterize changes in the particle size distribution of the studied systems.

2.4. Rheometry

The rheological behavior of the aqueous suspensions of PMS prepared using the initial commercial hydrogel ($C_{PMS} = 10$ wt%) diluted by twice-distilled deionized water to $C_{PMS} = 1, 3$, and 5 wt% was studied with increasing shear rate from 0.1 to 1312 s^{-1} and then its decrease to 0.1 s^{-1} at 293 K using a Rheotest 2.1 (VEB MLW Prufgerate-Werk Medingen Sitz Ftreital, Germany) rotational viscometer with a cylindrical measuring system.

The distribution function of activation energy $f(E)$ of the shear viscosity was determined using an integral equation derived for concentrated systems [49],

$$\eta(T, \dot\gamma) = \eta_\infty + (\eta_0 - \eta_\infty) \int_{E_{min}}^{E_{max}} \frac{1}{z} \int_0^z \frac{dx}{\sqrt{1+x^2}} f(E)\, dE, \tag{5}$$

where η_0 and η_∞ are the viscosity at the shear rates $\dot\gamma \to 0$ and $\dot\gamma \to \infty$, respectively, E_{min} and E_{max} are the limits of integration, and

$$z = \beta'\dot{\gamma} = c\dot{\gamma}\frac{a^2}{D_0}\frac{k_B T}{E}\exp\left(\frac{E}{k_B T}\right) = A\dot{\gamma}\frac{k_B T}{E}\exp\left(\frac{E}{k_B T}\right), \quad (6)$$

where c is a proportionality constant related to the network structure, a is the particle radius, D_0 is translational diffusion coefficient, k_B is the Boltzmann constant, T is the temperature, E is the activation energy, and A is a constant. Solution of Eq. (5) is a well-known ill-posed problem due to the impact of noise on measured data, which does not allow one to utilize exact inversion formulas or iterative algorithms. Therefore, Eq. (5) can be solved using a regularization procedure based on the CONTIN algorithm [47] under the condition of nonnegativity of $f(E) \geqslant 0$ at any E and fixed or unfixed regularization parameter determined by statistical analysis of the experimental data [47].

2.5. Nitrogen adsorption

To analyze the structural characteristics of unmodified and modified silicas (Tables 1 and 2), low-temperature (77.4 K) nitrogen adsorption–desorption isotherms were recorded using a Micromeritics ASAP 2405N adsorption analyzer. Before the measurements, unmodified silicas were degassed at 473 K for 2 h and modified silicas were degassed at 393 K for 2 h. The specific surface area (S_{BET}) was calculated according to the standard BET method [50]. The total pore volume V_p was evaluated by converting the volume of nitrogen adsorbed at $p/p_0 \approx 0.98$–0.99 (p and p_0 denote the equilibrium pressure and the saturation pressure of nitrogen at 77.4 K, respectively) to the volume of liquid nitrogen per gram of adsorbent. The nitrogen desorption data were utilized to compute pore size distributions (PSDs) (differential $f_V(R_p) \sim dV_p/dR_p$) using a modified regularization procedure under a nonnegativity condition ($f_V(R_p) \geqslant 0$ at any R_p) at a fixed regularization parameter $\alpha = 0.01$ [34–36,43–45,51,52]. For a pictorial presentation of the pore size distributions, the $f_V(R)$ functions were recalculated to incremental PSDs (IPSDs),

$$\Phi(R_{p,i}) = 0.5\big(f_V(R_{p,i}) + f_V(R_{p,i-1})\big)(R_{p,i} - R_{p,i-1}). \quad (7)$$

The specific surface area (S_φ) of nanosilica consisting of nonporous spherical nanoparticles can be calculated with the equation (derived on the basis of an equation from [53])

$$S_\varphi = \int_{a_{min}}^{a_{max}} \frac{3}{2a^3\rho}\Bigg[2(a+t)^2 + Nr_m \arcsin\left(\frac{a}{a+t+r_m}\right)\sqrt{(a+t+r_m)^2 - a^2} - N(a+t)\left(\frac{ar_m}{a+t+r_m} + t\right)\Bigg]\varphi(a)\,da, \quad (8)$$

where a is the particle radius, ρ is the material density, N is the average coordination number of primary particles in aggregates, t is the thickness of an adsorbed nitrogen layer, r_m is the meniscus radius corresponding to radius of void between spherical particles, and $\varphi(a)$ is the particle size distribution (calculated using the self-consisting regularization for $f_V(R)$ and $\varphi(a)$ with the model of voids between spherical nanoparticles) at t and r_m calculated at $0.05 < p/p_0 < 0.2$.

The PSDs were also calculated using the overall equation (with the framework of density functional theory, DFT) [54]

$$W(p) = v_M\left[\int_{\sigma_{ss}/2}^{r_k(p)} \rho_f(R) f(R)\,dR + \int_{r_k(p)}^{R_{max}} \frac{t}{R - \sigma_{ss}/2}\rho_M(R) f(R)\,dR\right], \quad (9)$$

where W is the adsorption and v_M is the liquid molar volume, ρ_f is the fluid density in occupied pores, ρ_m is the density of the multilayered adsorbate in pores, r_k the half-width of the pore filled at the pressure p, and σ_{ss} is the collision diameter of the surface atoms. To calculate the nitrogen density at a given pressure p, the generalized Bender equation [55,56] was used. Transition from gas to liquid or fluid in the form of a multilayered adsorbate in pores was determined using the corresponding equations for the fugacity [46].

To better describe the porosity of the studied samples, an additional regularizer was derived using the maximum entropy principle [48] applied to the distribution function $f_V(R_p)$. This procedure was used to modify the CONTIN algorithm to a self-consisting regularization procedure (CONTIN/MEM) with an unfixed regularization parameter to better fit the isotherms.

2.6. Thermally stimulated depolarization current (TSDC)

The tablets (diameter 30 mm, thickness ~1 mm) with frozen suspensions of unmodified and modified silicas were polarized by the electrostatic field at the intensity $F_p = 0.15$–0.35 MV/m at 260 K, cooled to 90 K with the field still applied, and heated without the field at the heating rate $\beta = 0.05$ K/s. The current evolved due to sample depolarization [42] was recorded by an electrometer over the range 10^{-15}–10^{-7} A. Relative mean errors for measured TSD current were $\delta_I = \pm 5\%$, $\delta_T = \pm 2$ K for temperature, and $\delta_\beta = \pm 5\%$ for the temperature change rate.

A modified Eq. (2) with k as a function of temperature T and pore radius R results in

$$k(T, R) = (1.77049 + 0.153T)\left(1 + \frac{1}{1+R}\right)\ [\text{K nm}] \quad (10)$$

at T between 90 and 273 K was used in the form of an integral equation (IGT) in estimation of IPSD (as a size distribution of relaxing water structures) on the basis of the TSDC data [42],

$$I(T_r) = A'\int_{R_{min}}^{R_{max}} \left(\frac{k(T, R)}{(T_{m,\infty} - T_r(R))R}\right)^2 f_V(R)\,dR, \quad (11)$$

where I is the TSD current, R_{max} and R_{min} the maximal and minimal pore radii (or sizes of relaxed water structures), respectively, $T_r(R)$ the temperature of relaxation of water (ice) structures in pores of radius R, and A' a normalization factor. The IGT equation (11) was solved using the CONTIN or CONTIN/MEM procedure.

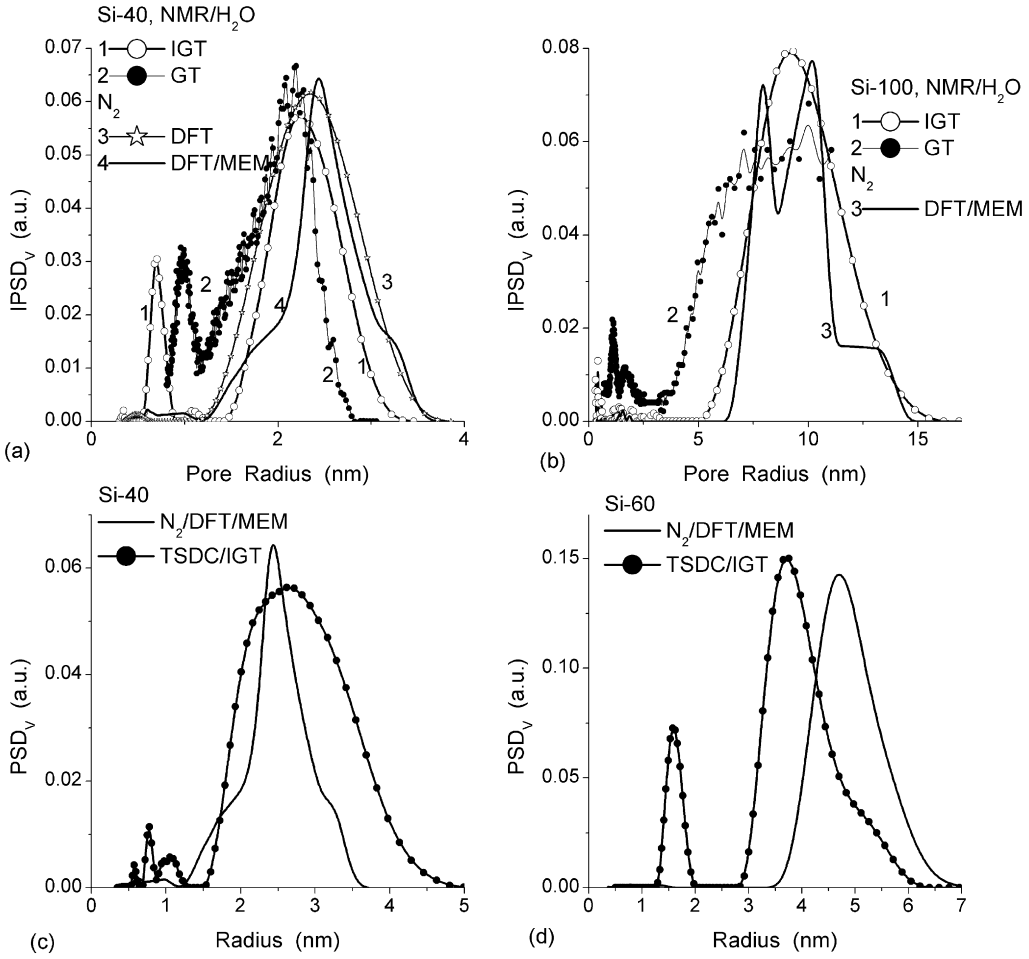

Fig. 1. Pore size distributions of silica gels (a, c) Si-40; (b) Si-100; and (d) Si-60 calculated on the basis of the nitrogen adsorption/desorption isotherms (labeled N_2), NMR (GT equation (1) and IGT equation (2)), and TSDC (IGT equation (11)).

2.7. Adsorption of albumin and gelatin

An aqueous solution (0.6 wt%) of a protein (ovalbumin, gelatin) and 0.2 g of PMS ($C_{PMS} = 10$ wt%) or 0.02 g of fumed silica A-300 was mixed for 1 h and then centrifuged. The equilibrium concentration of protein in the liquid was determined by the Biuret method [57–59].

A distribution function $f(-\Delta G)$ of Gibbs free energy (ΔG) for the protein adsorption was calculated using the Langmuir equation (modified to consider the lateral interaction between adsorbed molecules as described in detail elsewhere [60])

$$\Theta = \frac{bc}{1+bc}, \tag{12}$$

where $b = e^{-(\Delta G+z)/R_gT}$, $c = c_{eq}$ is the equilibrium gelatin concentration, and R_g is the gas constant, with regard to lateral interactions ($z = 2R_gT$) between adsorbed molecules. The right-hand term of Eq. (12) was used as the kernel in the overall adsorption equation in the form of a Fredholm integral equation of the first kind,

$$\Theta(T, C_{eq}) = \int_{-\Delta G_{min}}^{-\Delta G_{max}} \Theta_l(T, C_{eq}, \Delta G)\, f(-\Delta G)\, d(-\Delta G). \tag{13}$$

Equation (13) was solved using the modified regularization procedure CONTIN [47,61] under the nonnegativity condition $f(-\Delta G) > 0$ at any $-\Delta G$ values and the fixed regularization parameter $\alpha = 0.01$.

3. Results and discussion

3.1. Examination of GT and IGT equations

Application of NMR and TSDC cryoporometry with both GT and IGT equations to silica gels gives PSDs similar to those calculated on the basis of the nitrogen adsorption/desorption isotherms (Fig. 1). Both cryoporometry methods also show the formation of unfrozen (NMR) or relaxing (TSDC) water structures (<1–2 nm) smaller than the pore size. This can be due to the difference in conditions of freezing (relaxing) of pore water (ice) near the pore walls (occurring at lower temperatures) and in the centers of pores (occurring at higher temperatures) [33]. The observed similarity in the mentioned PSDs allowed us to use cryoporometry methods for the structural characterization of different materials in the aqueous media [33,42,45,46] as well as silicas and PMS studied here (Tables 1 and 2). This is of importance because removal of water can damage the structure of soft materials such as PMS hydrogel.

Table 1
Structural characteristics of dry powders and suspensions with fumed silica A-380 and differently silylated A-380 determined from the ^{1}H NMR data (γ_S, C_{uw}, and structural characteristics S and V with subscript IGT) and nitrogen adsorption/desorption isotherms

Parameter	A-380*	S1	S2	S3	S4	S5	S6
C_{TMS} (mmol/g)	0	0.09	0.14	0.12	0.23	0.42	0.79
S_{BET} (m^2/g)	378	379	362	372	345	330	285
S_{IGT} (m^2/g)	208	344	284	256	227	284	177
V_p (cm^3/g)	0.943	0.945	1.372	0.943	0.877	0.968	0.788
V_{IGT} (cm^3/g)	1.221	1.092	0.791	0.714	0.609	0.685	0.630
$S_{mic,IGT}$ (m^2/g)	–	168	166	140	137	158	73
S_{mes} (m^2/g)	317	325	270	318	256	274	246
$S_{mes,IGT}$ (m^2/g)	208	176	118	116	90	126	105
S_{mac} (m^2/g)	61	54	92	54	49	56	39
$V_{mic,IGT}$ (cm^3/g)	–	0.080	0.079	0.067	0.066	0.077	0.035
V_{mes} (cm^3/g)	0.456	0.450	0.424	0.438	0.413	0.416	0.385
$V_{mes,IGT}$ (cm^3/g)	1.168	0.916	0.626	0.601	0.477	0.589	0.542
V_{mac} (cm^3/g)	0.487	0.495	0.948	0.505	0.464	0.552	0.403
γ_S (J/g)	60.0	63.3	47.0	51.6	44.5	51.9	36.0
C_{uw} (mg/g)	1221	1092	791	714	609	685	630

Note. *$C_{OH} \approx 0.9$ mmol/g. S_{mic} and V_{mic} at $R < 1$ nm, S_{mes} and V_{mes} at $1 < R < 25$ nm, S_{mac} and V_{mac} at $R > 25$ nm; γ_S is the modulus of the total changes in the Gibbs free energy of interfacial water; the V and S values with the IGT subscripts were determined with the IGT equation (2).

Table 2
Structural characteristics of dry powder with fumed silica A-300 and differently silylated A-300 determined from the nitrogen adsorption/desorption isotherms

Parameter	A-300	S1	S2	S3	S4	S5
C_{DMS} (mmol/g)	–	0.24	0.57	0.84	1.12	1.21
C_{OH} (mmol/g)	0.53	0.55	0.42	0.31	0.11	–
ρ_{bulk} (g/cm^3)	0.041	0.028	0.031	0.035	0.034	0.36
S_{BET} (m^2/g)	337	343	273	214	183	150
S_{φ}[a] (m^2/g)	334	319	272	220	178	137
S_{mes} (m^2/g)	303	295	243	178	156	126
S_{mac} (m^2/g)	34	48	30	36	27	24
V_p (cm^3/g)	0.714	0.925	0.652	0.626	0.527	0.429
V_{mes} (cm^3/g)	0.379	0.420	0.314	0.244	0.217	0.170
V_{mac} (cm^3/g)	0.335	0.505	0.338	0.382	0.310	0.259

[a] $N = 3$.

Hydrophobic functionalities at a silica gel surface change the amounts and the temperature behavior of bound water (Fig. 2a), which undergoes clusterization (Fig. 2b) leading to formation of small structures with weakly associated interfacial water characterized by the chemical shift of the proton resonance at $\delta_H = 1.2$–1.7 ppm [33] and large clusters with $\delta_H \approx 5$ ppm (Fig. 2c). Water dissolved in chloroform has $\delta_H = 1.7$ ppm; however, the content of this water is too small (because water

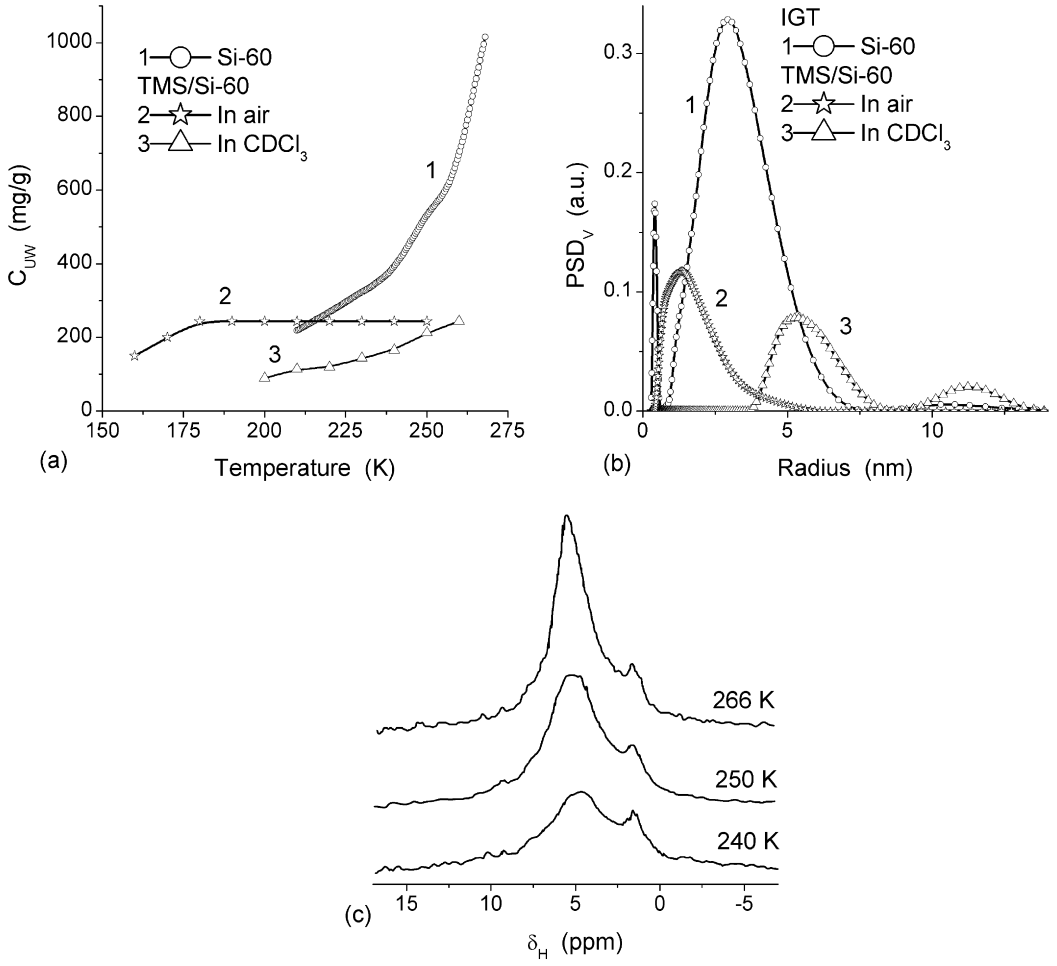

Fig. 2. (a) Temperature dependence of the content of unfrozen water for unmodified Si-60 (in air) and silylated Si-60 (in air and $CDCl_3$); (b) the corresponding distribution functions calculated using NMR cryoporometry with IGT equation (2); and (c) ^{1}H NMR spectra of water ($h = 0.244$ g of water per gram of dry modified silica) adsorbed on silylated Si-60 (in chloroform-d medium) at different temperatures.

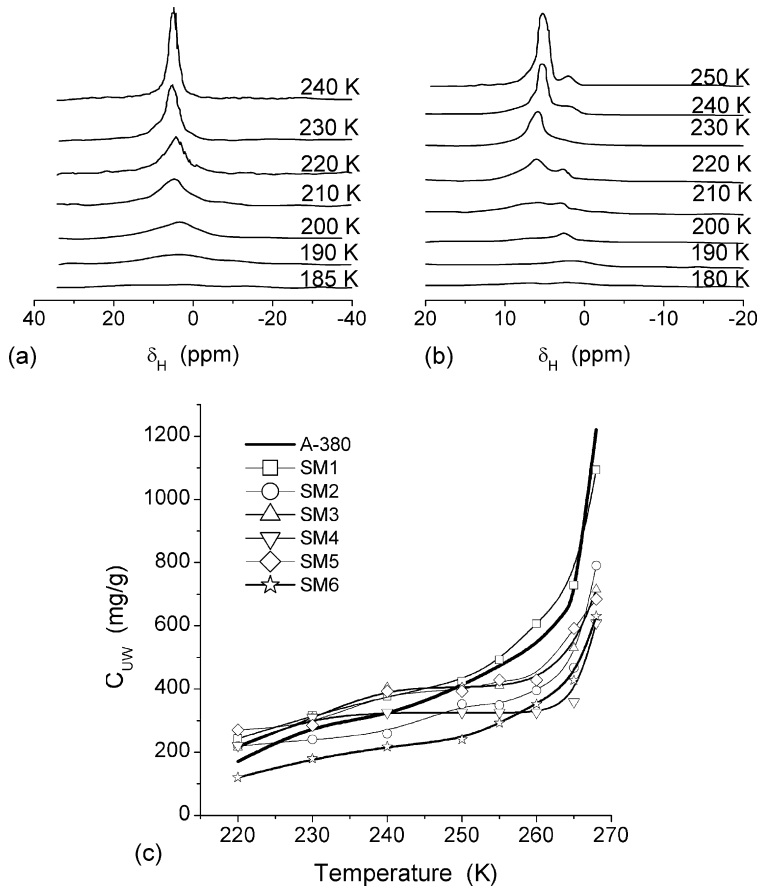

Fig. 3. ^{1}H NMR spectra of water adsorbed on SM1 ($h = 0.24$ g/g) in the presence of chloroform-d at (a) $C_{CDCl_3} = 0$ and (b) 0.6 g/g at different temperatures; and (c) temperature dependence of the amount of unfrozen water for unmodified and differently silylated fumed silicas (characteristics are shown in Table 1).

Table 3
Structural characteristics of wetted powders and suspensions with fumed silica A-300, silylated A-300 (DMS/A-300), and a mixture with 80 wt% of A-300 and 20 wt% of DMS/A-300 (Mix) determined from ^{1}H NMR data with Eq. (2)

Parameter	A-300	DMS/A-300	Mix	Mix	Mix	Mix	Mix
h (g/g)	17.0	17.0	0.092	0.182	0.332	4.0	17.0
S_{IGT} (m^2/g)	240	322	195	304	262	348	310
V_{IGT} (cm^3/g)	0.434	0.615	0.091	0.181	0.324	0.471	0.465
γ_S (J/g)	50.2	67.6	15.0	26.5	30.8	35.2	36.2

is poorly soluble in chloroform) to provide so intense a signal at the low δ_H value. Notice that similar unusual water appears in other systems with patchwise hydrophilic/hydrophobic structures [33]. Thus even partial (approximately 30%) silylation of silica gel Si-60 causes the formation of relatively small water clusters on incomplete filling of pores (Fig. 2b). This structured water is unfrozen at very low temperatures (Fig. 2a) and characterized by a low δ_H value. Replacement of the air medium with $CDCl_3$ leads to formation of larger water clusters frozen at higher temperatures because of the displacement of water from the surface and from the narrowest pores to larger ones by chloroform (Fig. 2b) to reduce the contact area between these immiscible liquids. Thus application of the IGT equation allows us to analyze rearrangement of pore water in silica gels depending on the pore structure (Fig. 1) or the surface modification and the presence of a weakly polar solvent (Fig. 2).

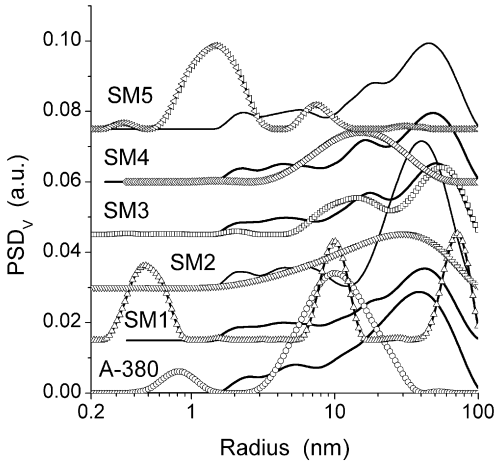

Fig. 4. Pore size distributions of unmodified and modified fumed silica A-380 (Table 1) calculated on the basis of the nitrogen adsorption/desorption isotherms using the DFT method with the model of pores as voids between spherical particles (lines) and NMR cryoporometry with IGT equation (2) (lines with symbols).

Silylation of nanosilica characterized by the textural porosity caused by voids between nanoparticles forming relatively soft secondary particles (aggregates and agglomerates) affects not only the behavior of structured water (Fig. 3) but also the structural characteristics of the material as a whole (Tables 1–3, Figs. 4–6). Calculation of the S_φ value (Table 2) shows that

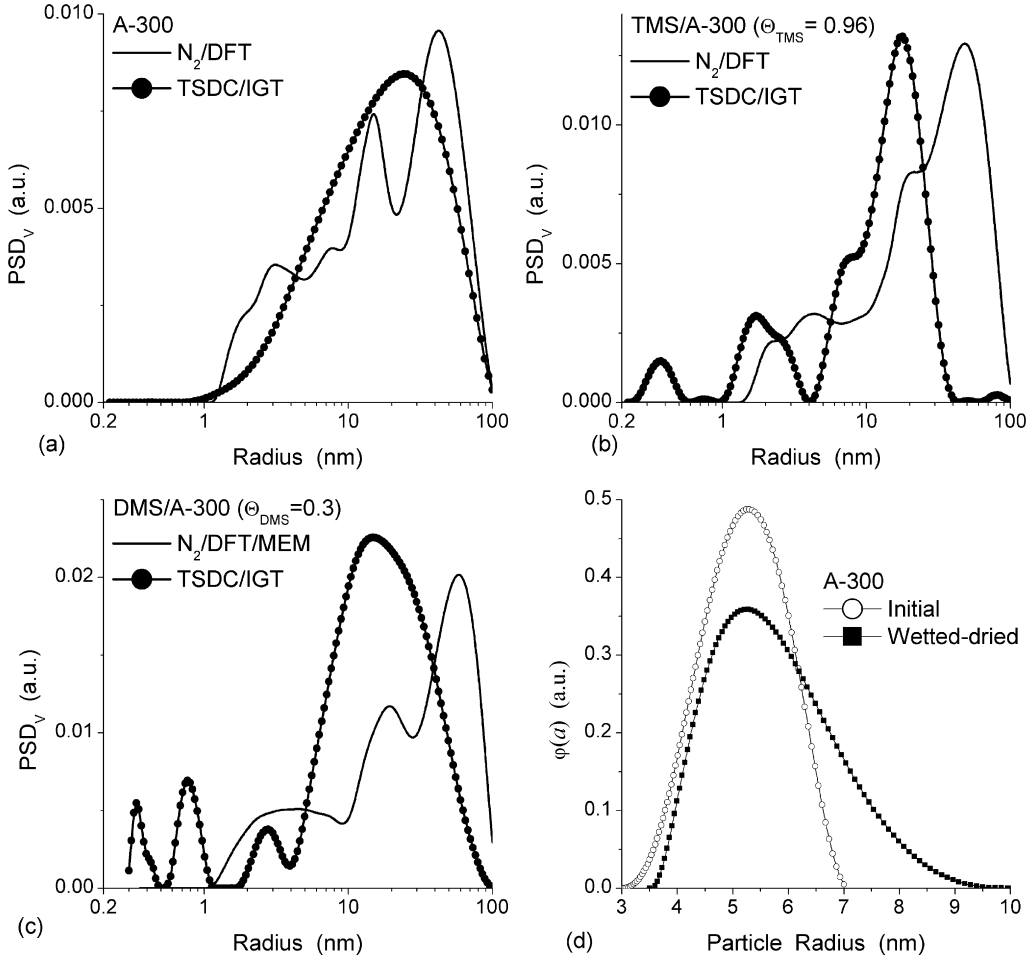

Fig. 5. Pore size distributions of unmodified and silylated fumed silica A-300 calculated on the basis of the nitrogen adsorption/desorption isotherm using DFT method with the model of pores as voids between spherical particles and TSDC cryoporometry with IGT equation (11): (a) initial A-300; (b) TMS/A-300; and (c) DMS/A-300; and (d) particle size distribution of initial and wetted/dried A-300.

it is close to the S_{BET} value at a low coordination number of primary particles in aggregates $N = 3$. This result and low values of the bulk density (ρ_{bulk}), i.e., the apparent density of the powders (Table 2), suggest nondense packing of primary silica particles. Estimation of the characteristics of micropores (S_{mic}, V_{mic}), mesopores (S_{mes}, V_{mes}), and macropores (S_{mac}, V_{mac}) (Tables 1 and 2) from the nitrogen adsorption shows predominant contribution of mesopores and macropores in this material. However, in the case of the aqueous suspensions, the contribution of micropores (which is close to zero for the powders) strongly increases for silylated samples (Table 1, $S_{mic,IGT}$ and $V_{mic,IGT}$). This may be due to the tendency to formation of the maximal number of contacts between silylated surface patches of neighboring particles to reduce their interaction with water.

Partial silylation of nanosilica leads to enhancement of clusterization of interfacial water (small structures in Figs. 4 and 5), which freezes at lower temperatures (Fig. 3), similar to that for silylated silica gel. The amounts of structured water (Table 1, C_{uw} and V_{IGT}) decrease for silylated silicas despite nearly the same adsorption capacity for adsorbed nitrogen (Table 1, V_p) because of reduction of the adsorption potential for water [33,34]. Enhancement of the clusterization of interfacial water is clearly observed from the PSD/IGT, especially for samples SM4 and SM5 (Fig. 4), since the PSDs shift toward smaller R values. Similar results are observed for silylated A-300 (Fig. 5) and a mechanical mixture of unmodified fumed silica A-300 and silylated A-300 with DMS functionalities (i.e., methylated silica, labeled as MS) (Fig. 6). The PSDs of unmodified A-300 and A-300-DMS/A-300 mixture are close. A decrease in hydration (h) leads to the appearance of small water clusters at $R < 1$ nm (Fig. 6a). Unmodified and silylated fumed silicas (Tables 1 and 2, Figs. 4 and 5) and the A-300-DMS/A-300 mixture (Fig. 6, Table 3) are mesoporous–macroporous materials; i.e., the size of the voids between particles is close or larger than the size of primary particles. Notice that wetting/drying of unmodified nanosilica leads to certain changes not only in the structure of secondary particles but also in that of the primary ones, which grow slightly (Fig. 5d). Clearly similar processes for PMS hydrogel can more strongly affect the structure of PMS particles.

3.2. PMS structures in hydrogel, suspension, and xerogel

Results obtained for unmodified and modified silicas using NMR and TSDC cryoporometry suggest that these techniques

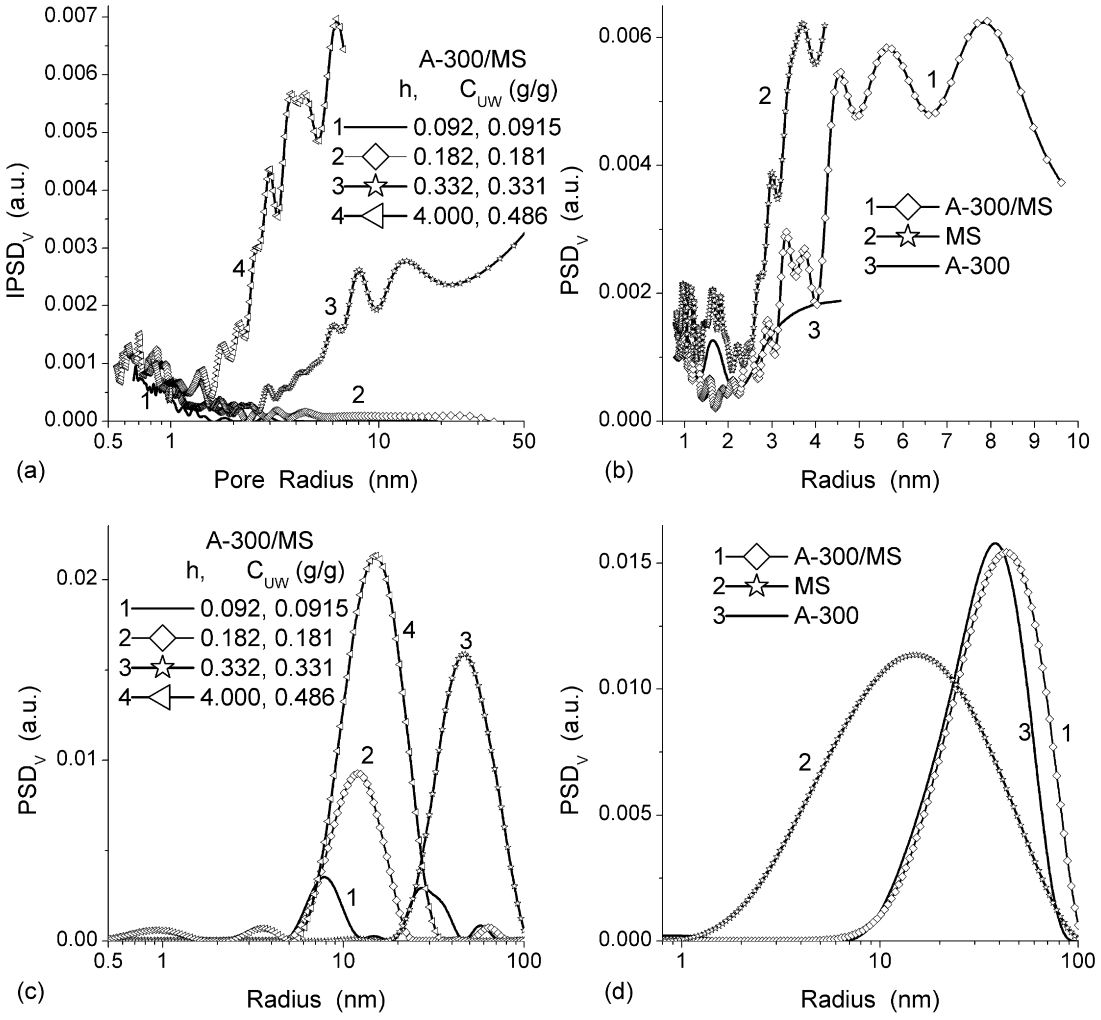

Fig. 6. PSDs of wetted powders (hydration $h = 0.092, 0.182$, and 0.332 g of water per gram of dry silica) and hydrogel ($h = 4$ g/g) of a mechanical mixture of unmodified silica A-300 and methylated A-300 (MS): (a, c) mechanical mixture of A-300 and MS; (b, d) A-300 and MS alone and its mixture calculated with the NMR cryoporometry using (a, b) GT (Eq. (1)) and (c, d) IGT (Eq. (2)) equations.

can be used to characterize the PMS hydrogel structure and the behavior of the interfacial water. The PMS macromolecules in the hydrogel are characterized by incomplete condensation of silanols because this material remains hydrophilic. Complete condensation of silanols leads to appearance of the hydrophobic properties of dried PMS xerogel because of the presence of CH_3 groups attached to each Si atom and very low content of residual hydrophilic silanols. PMS particles in the initial hydrogel ($C_{PMS} = 10$ wt%) or the aqueous suspensions ($C_{PMS} \leqslant 5$ wt%) can tend to form a continuous network to reduce the interaction of hydrophobic functionalities with water.

Information about the properties of the PMS hydrogel and suspensions can be obtained from a study of interfacial water by ^{1}H NMR spectroscopy with layer-by-layer freezing-out of bulk and structured bound water. The measurements of the ^{1}H NMR spectra were carried out in the deuterochloroform medium to accurately determine the value of the chemical shift of the proton resonance of interfacial water and to decrease the signal width [33]. Since deuterochloroform contained a small amount of tetramethylsilane (as an additive) used as the standard for the measurement of chemical shifts, the ^{1}H NMR spectra include not only the signal of unfrozen bound water but also signals of tetramethylsilane ($\delta = 0$ ppm) and the CH group of chloroform ($\delta = 7.26$ ppm) (Fig. 7). A signal observed at $\delta = 1.7$ ppm

Table 4
Structural characteristics of PMS hydrogels and dried/wetted xerogel determined from the ^{1}H NMR data with Eq. (2)

Parameter	C_{PMS} (wt%)				
	1.25	2.5	5.0	10.0	28.0
S_{IGT} (m^2/g)	177	243	201	197	225
$S_{IGT,mic}$ (m^2/g)	62	125	132	131	116
$S_{IGT,mes}$ (m^2/g)	115	108	64	65	104
$S_{IGT,mac}$ (m^2/g)	–	10	5	1	5
$V_{IGT,mic}$ (cm^3/g)	0.014	0.023	0.020	0.052	0.036
$V_{IGT,mes}$ (cm^3/g)	0.265	0.144	0.102	0.060	0.416
$V_{IGT,mac}$ (cm^3/g)	–	0.286	0.131	0.041	0.073
γ_S (J/g)	19.3	23.2	12.6	10.1	30.4
ΔG_s (kJ/mol)	−2.92	−3.71	−2.87	−3.44	−4.05
C_s (mg/g)	140	130	105	70	150
C_{uw} (mg/g)	280	454	259	153	527

Note. C_s and ΔG_s correspond to strongly bound water; IGT equation (2).

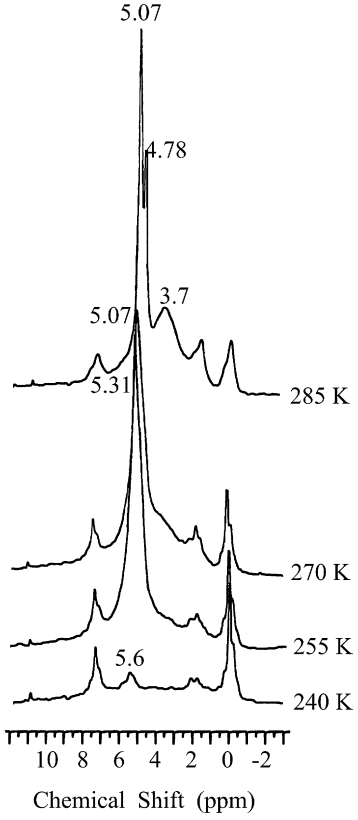

Fig. 7. ^{1}H NMR spectra of dried PMS xerogel recorded at different temperatures.

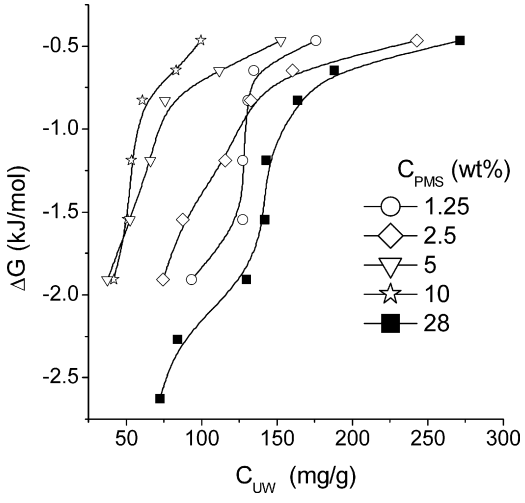

Fig. 8. Amounts of unfrozen water in differently hydrated PMS samples.

corresponds to weakly associated water, i.e., small water clusters that appear at a PMS surface with residual hydrophilic silanols and hydrophobic $SiCH_3$ groups [33]. The intensity of this signal decreases with decreasing temperature more slowly than that for other forms of interfacial water. The main signal at $\delta > 5$ ppm corresponds to strongly associated water, which freezes at $T < 255$ K. Water with the signal $\delta = 3.7$ ppm at 285 K can be attributed to weakly bound water, which freezes at T close to 273 K. The amount of this water is lower than that with $\delta > 5$ ppm because of low hydration ($h \approx 0.03$ g/g) of dry

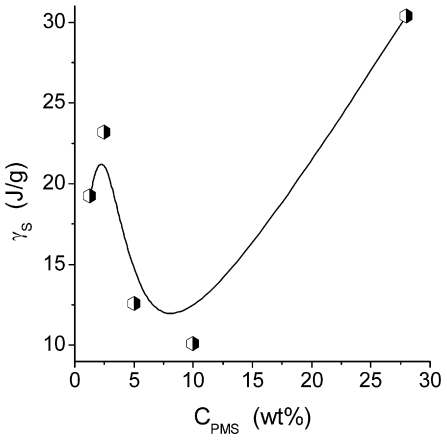

Fig. 9. Interfacial energy as a function of PMS concentration in the PMS/water systems.

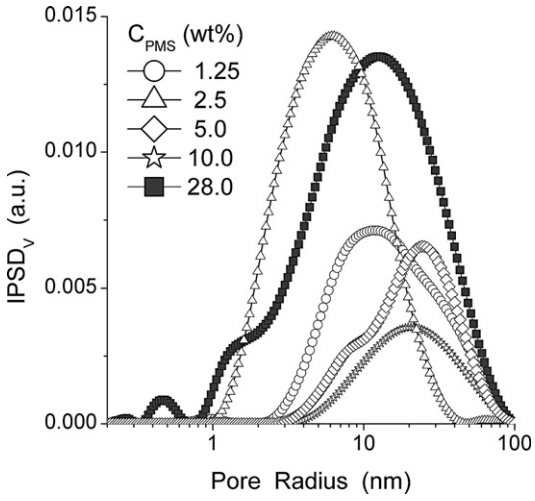

Fig. 10. PSDs of differently hydrated PMS samples.

PMS xerogel. PMS particles do not have a dense 3D bond network; therefore the presence of intraparticle water is possible in the form of relatively small clusters between residual silanols and $SiCH_3$ groups. This water can be responsible for the signal at $\delta = 1.7$ ppm. Water characterized by the signal at 5 ppm can be located in relatively narrow mesopores. Water giving the signal $\delta = 3.7$ ppm can be located in macropores. The main portion of water in macropores can be frozen at 273 K. As a whole, the amounts of water unfrozen at $T < 273$ are relatively low in dry PMS xerogel (because $h \approx 0.03$ g/g).

Addition of water to the initial PMS hydrogel or its drying/wetting leads to rearrangement of particles, since both treatments lead to an increase in the amounts of structured interfacial water (Fig. 8) and the structural characteristics noticeably change (Table 4). The maximal amount of structured water is observed at a lower hydration of dried/wetted PMS xerogel ($C_{PMS} = 28$ wt%). The amounts of unfrozen water are relatively small for all PMS samples: $C_{uw} < 530$ mg per g of dry material (because of the mentioned mesoporous–macroporous structure of PMS and, therefore, the freezing of the main amounts of water at $T \approx 273$ K). The amounts of water structured by silylated fumed silica (Table 1) are larger than for

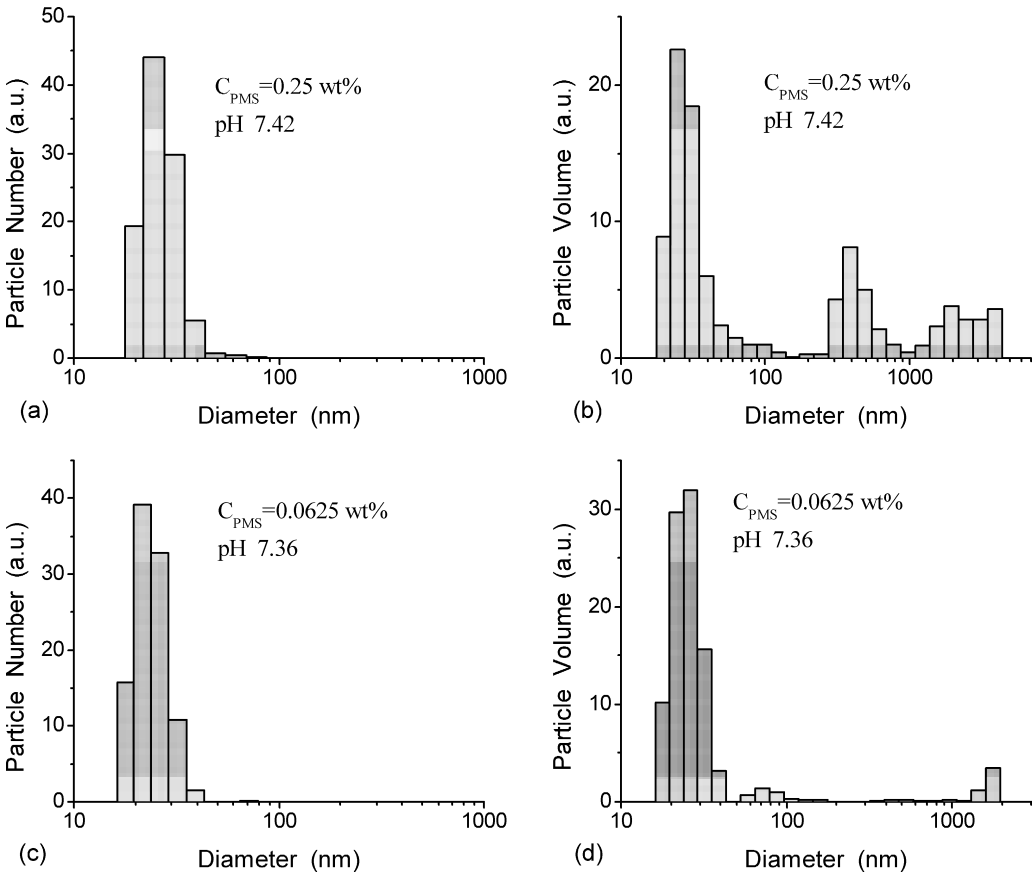

Fig. 11. Particle size distributions in the diluted aqueous suspensions of PMS at C_{PMS} = (a, b) 0.25 and (c, d) 0.0625 wt% shown with respect to (a, c) the particle number and (b, d) the particle volume.

PMS hydrogels. This may be due to a smaller surface area of PMS particles aggregated in secondary particles (which, however, can be destroyed on sonication). Additionally, silylation of any silica results in diminution of the adsorption potential for both nonpolar (e.g., nitrogen) and polar (water, polymers, proteins) compounds [33–36,63]. Therefore, PMS, which is similar to silylated nanosilica, is characterized by a low adsorption potential with respect to water. Therefore, the amounts of strongly bound water (Table 4, C_s) are smaller than that of weakly bound water (i.e., the difference $C_{uw} - C_s$). The corresponding changes in the surface energy (Fig. 9) show that the initial PMS hydrogel ($C_{PMS} = 10$ wt%) is characterized by the smallest γ_S value. In other words, the state of the initial PMS hydrogel is metastable, since changes in the water content in both directions lead to reduction of the Gibbs free energy of the system. The γ_S values for the PMS systems (Fig. 9) are smaller than that for unmodified silica and silylated A-380 (Table 1) or A-300 (Table 3) but close to that for the A-300–DMS/A-300 mixtures (Table 3). Notice that this mechanical mixture is metastable, as it strongly changes structure on addition of water, which leads to separation of the hydrophilic and hydrophobic components. Consequently, the metastable state of the PMS systems and the relatively high Gibbs free energy of the interface are caused by a patchwise hydrophobic–hydrophilic PMS structure.

Calculations of the size distribution of unfrozen water structures (Fig. 10) show that the initial material is the most compacted (V is minimal, Table 4) but the pore size filled by structured water is nearly maximal (peak maximum at $R = 22$ nm). It is also possible that the initial material is characterized by a smaller number of residual silanols than the diluted suspensions; therefore, its capability for the structurization of water is minimal. This capability increases on decomposition of the PMS particles, leading to an increase in the number of silanols, because some number of Si–O–Si bonds can be broken. The first diluted system ($C_{PMS} = 5$ wt%) has both broader (maximum at $R = 24$ nm) and narrower ($R = 8$ nm) pores. Subsequent dilution leads to formation of smaller water structures. This may be due to rearrangement of decomposed particles and formation of more comparted structures, since the suspension was stirred on dilution. The dilution of the hydrogel enhances its mesoporosity. Possibly micropores transform into mesopores, since an increase in the $S_{IGT,mes}$ and $V_{IGT,mes}$ values is accompanied by a decrease in the $S_{IGT,mic}$ and $V_{IGT,mic}$ values (Table 4) and the total surface area grows. These results can be explained by decomposition of PMS particles into smaller ones on the dilution of the initial PMS hydrogel and rearrangement of them into new secondary structures. Another type of rearrangement of particles occurs on drying of hydrogel to dry xerogel ($C_{PMS} \approx 97$ wt%), which is then wetted ($C_{PMS} = 28$ wt%) because of condensation of residual silanols. The narrowest pores at $R < 1$ nm are characteristic for this material; however, broad pores remain (Fig. 10). Consequently, the

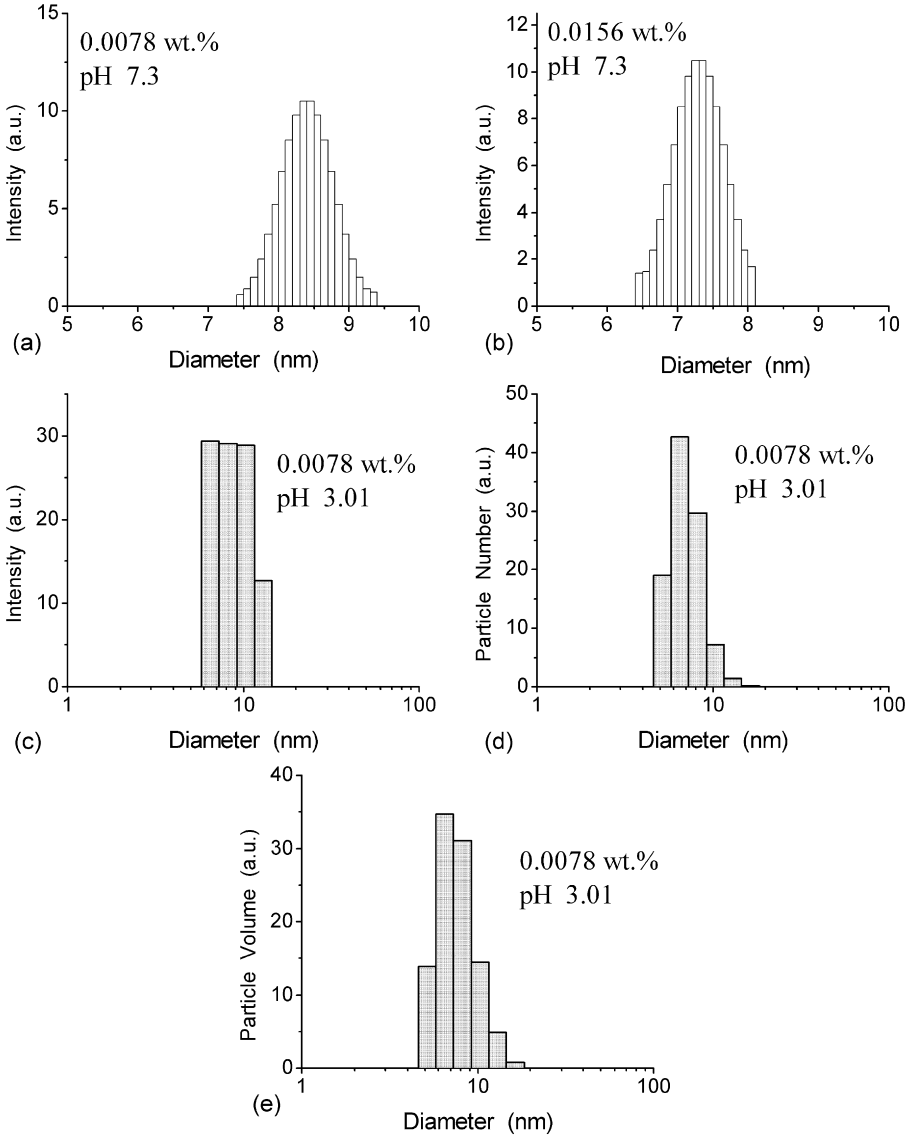

Fig. 12. Particle size distributions in the diluted aqueous suspensions of PMS at C_{PMS} = (a, c, d, e) 0.0078 and (b) 0.0156 wt% shown with respect to (a, b, c) intensity of scattered light; (d) particle number; and (e) particle volume at pH (a, b) 7.3 and (c, d, e) 3.01.

collapse of the textural pores does not occur on drying/wetting of PMS, despite the xerogel being hydrophobic due to strong reduction of the number of residual silanols.

3.3. QELS and rheometry of aqueous suspensions of PMS

The particle size distributions in the aqueous suspensions of PMS can be relatively broad (Fig. 11) or very narrow (Fig. 12) depending on concentration, pH value, and sonication time. It should be noted that the QELS intensity for PMS was less by an order of magnitude than that for the suspensions of fumed silica with the same concentration. This is due to the differences in the morphology of secondary PMS particles and in the nature of primary particles, because the 3D network in PMS particles is looser and close to the 2D network due to CH_3 groups attached to each Si atom and residual silanols. For maximally diluted PMS suspensions, a monodisperse particle distribution is characteristic, because this concentration is much smaller than that sufficient to form a continuous network with primary and secondary particles. The effective diameter of PMS particles, D_{eff}, does not change with decreasing PMS concentration at $C_{PMS} < 0.06$ wt% and it is equal to 7–8 nm. This particle size can be assumed to be that of primary PMS particles.

The rheological behavior of PMS suspensions was investigated to elucidate the influence of PMS concentration on interaction between particles. Diluted PMS hydrogel (i.e., suspension or colloidal solution) is characterized by the viscosity increasing with concentration (Fig. 13a). The distribution function of the activation energy of the shear viscosity shifts toward higher energy with increasing C_{PMS} value (Fig. 13b). The structure of the dispersion becomes more complex since the $f(E)$ function is multimodal at $C_{PMS} = 5$ wt%. The viscosity of the aqueous suspension of fumed silica even at higher concentration (8 wt%) is lower, since the $f(E)$ peak is at lower E values. Features of different interactions between colloidal particles of PMS or fumed silica determining the formation

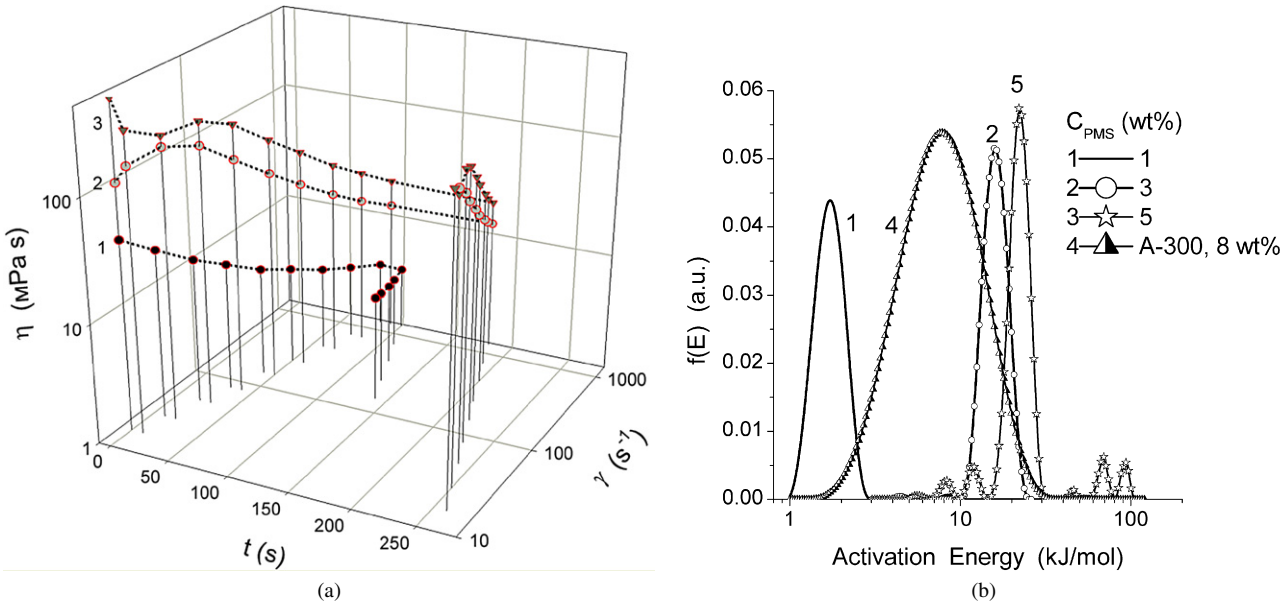

(a) (b)

Fig. 13. (a) Viscosity as a function of the shear rate and measurement time for aqueous suspensions of PMS at C_{PMS} = (1) 1; (2) 3; and (3) 5 wt%; and (b) corresponding distribution functions of activation energy of the shear viscosity ($f(E)$ is shown for the suspension of A-300 at 8 wt%).

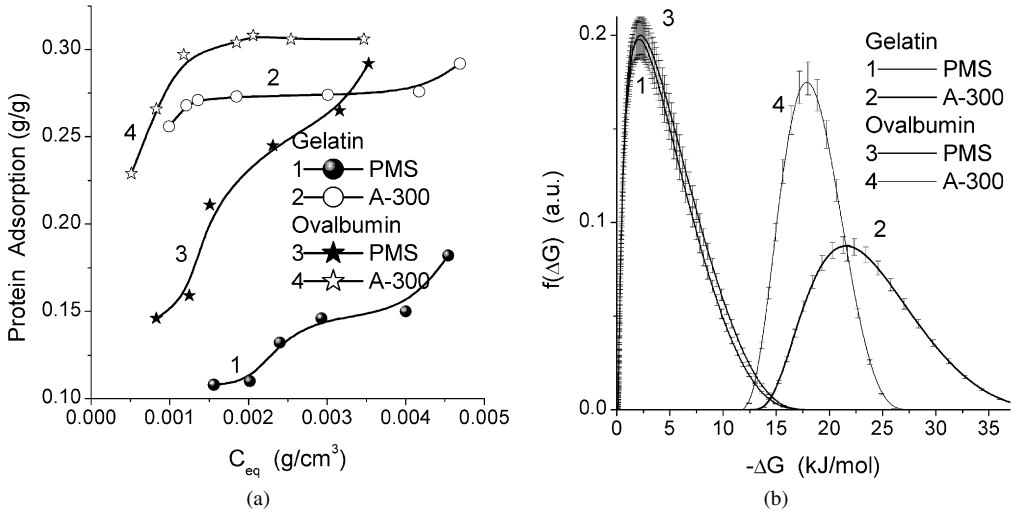

(a) (b)

Fig. 14. (a) Isotherms of adsorption of gelatin and ovalbumin onto PMS and fumed silica and (b) the corresponding distribution functions of the Gibbs free energy of protein adsorption.

of the 3D network with primary particles forming secondary ones in the dispersions may be responsible for this difference in the $f(E)$ functions. In rheological studies, destruction of secondary structures occurs, which is manifested in changes in the rheological parameters of the dispersions during the measurements. This destruction, which is progressive with increasing shear rate, is manifested in deviations of the characteristics from those for the Newtonian flow [62]. If the recovery rate of destroyed interparticle bonds does not exceed the rate of their destruction, then the viscosity decreases until the rates of both processes become equal one to one another. This equilibrium can be reached for a short time at $C_{PMS} = 1$ wt% (Fig. 13a, curve 1), which indicates a relatively low thixotropy of the system. An increase in the C_{PMS} value leads to an increase in the thixotropy (curves 2 and 3). The viscosity and the shear stress practically linearly depend on PMS concentration at the highest shear rate, $\dot{\gamma} = 1312\ s^{-1}$. The effect of an increase in the viscosity value on the measurements due to a higher rate of bond formation than of their destruction is not observed at different concentrations of PMS, although the viscosity is noticeably higher at smaller $\dot{\gamma}$ values and depends on C_{PMS}. These results suggest the absence of stable aggregates in the PMS suspensions, which is in agreement with the QELS data showing the monodispersity of the diluted suspensions and the rapid destruction of aggregates on sonication of the suspensions, although fast structurization can occur in the concentrated suspensions at $C_{PMS} \geqslant 3$ wt% because of aggregation of primary particles. The presence of aggregates and agglomerates at $C_{PMS} \geqslant 3$ wt% causes significant enhancement of the viscosity, especially at small $\dot{\gamma}$ values.

Thus, the diluted PMS suspensions have a practically monodisperse distribution of primary nanoparticles forming aggre-

gates and agglomerates (which can be easily destroyed) with increasing PMS concentration. Clearly the absence of stable aggregates and agglomerates plays an important role on applications of PMS as an enterosorbent [17,18], providing a relatively high rate of diffusion of primary particles in the liquid medium.

3.4. Adsorption of proteins

The comparative analysis of the adsorption of gelatin and ovalbumin on PMS and fumed silica A-300 shows that the adsorption capacity of PMS is lower than that of A-300 (Fig. 14a). The presence of $\equiv SiCH_3$ groups in PMS may be responsible for this effect. Notice that the difference in the adsorption of ovalbumin is higher than that for gelatin. However, the distribution functions of the Gibbs free energy of adsorption are similar for both proteins adsorbed onto PMS (Fig. 14b), since the difference in the peak position is smaller than 0.3 kJ/mol.

Diminution of the interaction of PMS with proteins in comparison with nanosilica can provide a higher biocompatibility of PMS particles. One can assume that, e.g., hemolysis of red blood cells (RBCs) caused by PMS can be much smaller than that caused by unmodified fumed silica, since nanosilica modified by immobilized polymers causes lower hemolysis of RBCs [63].

4. Conclusion

According to the results of NMR cryoporometry and QELS, PMS hydrogel can be classified as a mesoporous–macroporous material with mainly textural porosity caused by voids between nanosized primary particles, which are nondense and nonrigid because of the presence of CH_3 groups attached to each Si atoms and residual silanols. Consequently, PMS particles can be considered as strongly crumpled 2D sheets rather than 3D solid particles, because the $\equiv$Si–O–Si$\equiv$ linkages do not form the solid 3D network characteristic for silica. This structural feature of PMS causes the formation of three types of water structures: (i) very small intraparticle water clusters located inside primary PMS particles and characterized by the chemical shift of the proton resonance at $\delta_H \approx 1.7$ ppm corresponding to weakly associated but strongly bound water frozen at $T < 240$ K; (ii) interparticle water located close to the particle surface and forming larger clusters in mesopores (strongly associated and both strongly and weakly bound waters at $\delta_H \geqslant 5$ ppm) frozen at $T > 240$ K; and (iii) weakly bound water at $\delta_H \approx 3.7$ ppm located in macropores and frozen at T close to 273 K. Despite the soft character of secondary particles, the viscosity of the aqueous suspensions of PMS at $C_{PMS} = 3$–5 wt% is higher than that of the aqueous suspension of fumed silica A-300 at $C_{A\text{-}300} = 8$ wt%, because PMS particles tend to form a continuous network in the suspensions to reduce the interaction of hydrophobic $SiCH_3$ groups with water. Additionally, the initial PMS hydrogel at $C_{PMS} = 10$ wt% is not liquid, since it looks like nearly dry, soft, pastelike, and very thixotropic hydrogel (i.e., there is a continuous structure there), in contrast to the 10 wt% suspension of fumed nanosilica, which remains liquid for a very long time. The adsorption capacity of PMS with respect to proteins (gelatin, ovalbumin) is smaller than that of fumed silica despite close values of the specific surface area because of the effects of $\equiv SiCH_3$ functionalities in PMS reducing the adsorption potentials with respect to any adsorbate.

Acknowledgment

This research was supported by the National Academy of Sciences of Ukraine (Complex Program of Fundamental Investigations "Nanostructural Systems, Nanomaterials, and Nanotechnology").

References

[1] Conference on Electrical Insulation and Dielectric Phenomena (CEIDP), IEEE, Dielectrics and Electrical Insulation Society, 2000.
[2] J. Cordelair, P. Greil, J. Am. Ceram. Soc. 84 (2001) 2256.
[3] G.D. Sorarù, H.-J. Kleebe, R. Ceccato, L. Pederiva, J. Eur. Ceram. Soc. 20 (2000) 2509.
[4] R. Hooper, L.J. Lyons, D. Moline, R. West, Organometallics 17 (1999) 3249.
[5] M.K. Mapes, D. Schumacher, L.J. Lyons, D. Moline, R. Hooper, R. West, Polym. Preprints 41 (2000) 401.
[6] R. Hooper, L.J. Lyons, M.K. Mapes, D. Schumacher, D. Moline, R. West, Macromolecules 34 (2001) 931.
[7] R. Hooper, L.J. Lyons, D. Moline, R. West, Silicon Chem. 1 (2002) 121.
[8] J.J. Jin, L.J. Lyons, Q. Wang, R. West, Polym. Preprints 44 (2003) 1148.
[9] Z. Zhang, D. Sherlock, R. West, K. Amine, L.J. Lyons, Macromolecules 36 (2003) 9176.
[10] P. Taranekar, X. Fan, R. Advincula, Langmuir 18 (2002) 7943.
[11] Z. Zhang, S. Fang, Electrochim. Acta 45 (2000) 2131.
[12] G.A. Guiochon, L.A. Beaver, Anal. Chim. Acta 524 (2004) 1.
[13] H.H. Schmitz, W.E. Artz, C.L. Poor, J.M. Dietz, J.W. Erdman Jr., J. Chromatogr. A 479 (1989) 261.
[14] W.M.L. Chow, B. Caddy, J. Chromatogr. A 318 (1985) 255.
[15] M. Krogh, K. Johansen, F. Tønnesen, K.E. Rasmussen, J. Chromatogr. B 673 (1995) 299.
[16] O.M. Volpina, A.V. Yarov, M.N. Zhmak, M.A. Kuprianova, A.V. Chepurkin, A.S. Toloknov, V.T. Ivanov, Vaccine 14 (1996) 1375.
[17] Yu.N. Shevchenko, E.N. Gritsenko, V.A. Znamensky, T.V. Gerasimchuk, Pharmac. Zh. 5–6 (1994) 36.
[18] Yu.N. Shevchenko, I.B. Slinyakova, N.I. Yashina, Pharmac. Zh. 6 (1995) 80.
[19] J. Sun, H. Tang, J. Jiang, P. Xie, R. Zhang, P.-F. Fu, Q. Wu, Polymer 44 (2003) 2867.
[20] N. Garti, A. Aserin, E. Wachtel, O. Gans, Y. Shaul, J. Colloid Interface Sci. 233 (2001) 286.
[21] Y. Shirai, K. Kawatsura, N. Tsubokawa, Prog. Org. Coat. 36 (1999) 217.
[22] T. Suhara, T. Kanemaru, H. Fukui, M. Yamaguchi, Colloids Surf. A 95 (1995) 1.
[23] H.G. Alt, P. Schertl, A. Köppl, J. Organomet. Chem. 568 (1998) 263.
[24] V. Percec, D. Tomazos, Polymer 31 (1990) 1658.
[25] M. Mauzac, F. Hardouin, H. Richard, M.F. Achard, G. Sigaud, H. Gasparoux, Eur. Polym. J. 22 (1986) 137.
[26] V.M. Litvinov, B.D. Lavrukhin, A.A. Zhdanov, Polym. Sci. USSR 27 (1985) 2777.
[27] B.B. Badmaev, U.B. Bazaron, B.V. Derjaguin, O.R. Budaev, Physica B + C 122 (1983) 241.
[28] I.B. Slinyakova, T.I. Denisova, Organosilicon Adsorbents: Preparation and Properties, Naukova Dumka, Kiev, 1988.
[29] R.H. Gee, R.S. Maxwell, B. Balazs, Polymer 45 (2004) 3885.
[30] L.N. Dinh, M.A. Schildbach, R.S. Maxwell, W.J. Siekhaus, B. Balazs, W. McLean II, J. Colloid Interface Sci. 274 (2004) 25.

[31] H.E. Bergna (Ed.), Colloidal Silica: Fundamentals and Applications, Taylor & Francis, Salisbury, 2005.
[32] A.T. Hubbard (Ed.), Encyclopedia of Surface and Colloid Science, Dekker, New York, 2002.
[33] V.M. Gun'ko, V.V. Turov, V.M. Bogatyrev, V.I. Zarko, R. Leboda, E.V. Goncharuk, A.A. Novza, A.V. Turov, A.A. Chuiko, Adv. Colloid Interface Sci. 118 (2005) 125.
[34] V.M. Gun'ko, V.I. Zarko, D.J. Sheeran, S.M. Augustine, J.P. Blitz, Adsorption 11 (2005) 703.
[35] V.M. Gun'ko, V.V. Turov, V.M. Bogatyrev, B. Charmas, J. Skubiszewska-Zięba, R. Leboda, S.V. Pakhovchishin, V.I. Zarko, L.V. Petrus, O.V. Stebelska, M.D. Tsapko, Langmuir 19 (2003) 10816.
[36] V.V. Turov, V.M. Gun'ko, M.D. Tsapko, V.M. Bogatyrev, J. Skubiszewska-Zięba, R. Leboda, J. Riczkowski, Appl. Surf. Sci. 229 (2004) 197.
[37] V.M. Gun'ko, V.I. Zarko, R. Leboda, E. Chibowski, Adv. Colloid Interface Sci. 91 (2001) 1.
[38] V.M. Gun'ko, A.V. Klyueva, Yu.N. Levchuk, R. Leboda, Adv. Colloid Interface Sci. 105 (2003) 201.
[39] J.H. Strange, M. Rahman, E.G. Smith, Phys. Rev. Lett. 71 (1993) 3589.
[40] J.H. Strange, J. Mitchell, J.B.W. Webber, Magn. Reson. Imag. 21 (2003) 221.
[41] D.W. Aksnes, L. Kimtys, Solid State Nucl. Magn. Reson. 25 (2004) 146.
[42] V.M. Gun'ko, V.I. Zarko, E.V. Goncharuk, L.S. Andriyko, V.V. Turov, Y.M. Nychiporuk, R. Leboda, J. Skubiszewska-Zięba, A.L. Gabchak, V.D. Osovskii, Y.G. Ptushinskii, G.R. Yurchenko, O.A. Mishchuk, P.P. Gorbik, P. Pissis, J.P. Blitz, Adv. Colloid Interface Sci., in press.
[43] V.M. Gun'ko, J. Skubiszewska-Zieba, R. Leboda, V.V. Turov, Colloids Surf. A 235 (2004) 101.
[44] V.M. Gun'ko, V.V. Turov, J. Skubiszewska-Zięba, B. Charmas, R. Leboda, Adsorption 10 (2004) 5.
[45] V.M. Gun'ko, V.V. Turov, A.V. Turov, V.I. Zarko, V.I. Gerda, V.V. Yanishpolskii, I.S. Berezovska, V.A. Tertykh, Central Eur. J. Chem., in press.
[46] V. M. Gun'ko, V. V. Turov, R. Leboda, V. I. Zarko, J. Skubiszewska-Zięba, B. Charmas, Langmuir, in press.
[47] S.W. Provencher, Comput. Phys. Commun. 27 (1982) 213.
[48] W.B. Muniz, F.M. Ramos, H.F. de Campos Velho, Comput. Math. Appl. 40 (2000) 1071.
[49] V.M. Gun'ko, E.V. Goncharuk, O.V. Nechypor, S.V. Pakhovchishin, V.V. Turov, J. Colloid Interface Sci. 304 (2006) 239.
[50] S. Brunauer, P.H. Emmett, E. Teller, J. Am. Chem. Soc. 60 (1938) 309.
[51] V.M. Gun'ko, V.I. Zarko, E.F. Voronin, V.V. Turov, I.F. Mironyuk, I.I. Gerashchenko, E.V. Goncharuk, E.M. Pakhlov, N.V. Guzenko, R. Leboda, J. Skubiszewska-Zięba, W. Janusz, S. Chibowski, Yu.N. Levchuk, A.V. Klyueva, Langmuir 18 (2002) 581.
[52] V.M. Gun'ko, I.F. Mironyuk, V.I. Zarko, E.F. Voronin, V.V. Turov, E.M. Pakhlov, E.V. Goncharuk, Yu.M. Nychiporuk, T.V. Kulik, B.B. Palyanytsya, S.V. Pakhovchishin, N.N. Vlasova, P.P. Gorbik, O.A. Mishchuk, A.A. Chuiko, J. Skubiszewska-Zięba, W. Janusz, A.V. Turov, R. Leboda, J. Colloid Interface Sci. 289 (2005) 427.
[53] S.J. Gregg, K.S.W. Sing, Adsorption, Surface Area and Porosity, second ed., Academic Press, London, 1982.
[54] D.D. Do, C. Nguyen, H.D. Do, Colloids Surf. A 187–188 (2001) 51.
[55] B. Platzer, G. Maurer, Fluid Phase Equilibr. 51 (1989) 223.
[56] B. Platzer, G. Maurer, Fluid Phase Equilibr. 84 (1993) 79.
[57] V.V. Menshikov (Ed.), Laboratory Investigation Methods in Clinic Medicine, Vysshaya Shkola, Moscow, 1987.
[58] T. Weichselbaum, Am. J. Clin. Pathol. 16 (1946) 40.
[59] G.A. Kochetov, Practical Enzymology Manual, Vysshaya Shkola, Moscow, 1980.
[60] A.W. Adamson, A.P. Gast, Physical Chemistry of Surface, sixth ed., Wiley, New York, 1997.
[61] V.M. Gun'ko, V.I. Zarko, E.F. Voronin, E.V. Goncharuk, L.S. Andriyko, N.V. Guzenko, L.V. Nosach, W. Janusz, J. Colloid Interface Sci. 300 (2006) 20.
[62] N.B. Ur'ev, Kolloid Zh. 60 (1995) 662.
[63] J.P. Blitz, V.M. Gun'ko (Eds.), Surface Chemistry in Biomedical and Environmental Science, in: NATO Science Series II: Mathematics, Physics and Chemistry, vol. 228, Springer-Verlag, New York, 2006.